Scientific Research Publishing

Journal of Geoscience and Environment Protection, 2024, 12, 162-175
https://www.scirp.org/journal/gep
ISSN Online: 2327-4344
ISSN Print: 2327-4336

Characteristics of *In-Situ* Soil Water Hysteresis Observed through Multiple-Years Monitoring

Ippei Iiyama

School of Agriculture, Utsunomiya University, Utsunomiya, Japan
Email: iiyama@cc.utsunomiya-u.ac.jp

How to cite this paper: Iiyama, I. (2024). Characteristics of *In-Situ* Soil Water Hysteresis Observed through Multiple-Years Monitoring. *Journal of Geoscience and Environment Protection, 12,* 162-175.
https://doi.org/10.4236/gep.2024.125010

Received: March 25, 2024
Accepted: May 25, 2024
Published: May 28, 2024

Abstract

A soil water retention curve (SWRC) is an essential soil physical property for analyzing transport and retention of water in a soil layer. A SWRC is often described as a single-valued function that relates the soil water potential ψ to volumetric water content θ of the soil. However, an *in-situ* $\psi - \theta$ relation should show soil water hysteresis, though this fact is often neglected in analyses of field soil water regimes while long-term *in-situ* soil water hysteresis is not well characterized. This study aimed at probing and characterizing *in-situ* $\psi - \theta$ relations. The developments of large hysteresis in the *in-situ* $\psi - \theta$ relations were observed only a few times during the study period of 82 months. Any of the large hysteretic behaviors in the $\psi - \theta$ relations began with an unusually strong continual reduction in ψ. The completion of a hysteresis loop required a recorded maximum rainfall. Because the study field had very small chances to meet such strong rainfall events, it took multiple years to restore the fraction of soil water depleted by the unusually strong continual reduction in ψ. While wetting-drying cycles had occurred within a certain domain of ψ, hysteretic behaviors tended to be so small that the *in-situ* $\psi - \theta$ relation can be approximated as a single-valued function of $\theta(\psi)$. These observed patterns of the *in-situ* $\psi - \theta$ relations were characterized by kinds of difference in $d\theta/d\psi$ between a drying process and a wetting process at a given ψ. Thus, more amounts of experimental facts about wetting SWRCs in parallel with drying SWRCs should be needed for correct modelling, analyzing, and predicting soil water regimes in fields. It is also necessary to increase our understandings about the long-term trends of occurrences of extreme weather conditions associated with possible change in climate.

Keywords

Atmospheric Conditions, Field Water Regimes, Hysteretic Behaviors, Soil Moisture Conditions, Soil Water Characteristic Curves, Specific Water Capacity, Wetting-Drying Cycles

1. Introduction

A soil water retention curve (SWRC) is a relationship between the soil water potential ψ and volumetric water content θ of the soil. Mathematical features of SWRC have been used for classifying soil water in terms of energy state or plant-availability (Veihmeyer & Hendrickson, 1931; Hoover, 1950; Richards & Weaver, 1943; Veihmeyer & Hendrickson, 1948). A SWRC can also allow to infer pore size distribution of a soil based on the theoretical relation between pore water pressure and radius of capillary pores (Washburn, 1921). The concept of specific water capacity $\mathrm{d}\theta/\mathrm{d}\psi$ is another aspect of the pore size distribution given by a SWRC, indicating how a soil is apt to dry or wet with the change in ψ under a certain moisture condition.

A SWRC is, thus, mostly described by a single-valued continuous function $\theta(\psi)$ for the convenience of the evaluation works mentioned above. Common procedures to obtain a $\theta(\psi)$ are laboratory tests using hanging-water columns or pressure-plate apparatuses (Dane & Hopmans, 2002). Most of such procedures rely on a drying process through which water is removed from an initially saturated soil sample by increasing suction on water in the soil sample step by step. After the procedure gives a series of $\psi - \theta$ plots, a mathematical function of $\theta(\psi)$ is fitted to the measured $\psi - \theta$ plots so that the parameters in the expression of the $\theta(\psi)$ are identified. Classical studies that proposed mathematical functions for describing SWRCs are Campbell (1974), Clapp and Hornberger (1978), and van Genuchten (1980). Once a $\theta(\psi)$ is identified, it can be used to typify a $\psi - \theta$ relation that would be observed for the soil in question.

However, a series of $\psi - \theta$ plots, or a $\psi - \theta$ relation, in a field may not be appropriately formulated by a single-valued function, because the field soil is incessantly experiencing wetting-drying cycles so that its $\psi - \theta$ relation may vary, which is known as soil water hysteresis (Hillel, 1998; Kutilek & Nielsen, 1994). Soil water hysteresis was first discussed by Haines (1930), and was later explained by the analogy named the "ink-bottle effect". The ink-bottle effect can occur due to varying pore-diameter along a capillary pore, causing the difference in soil water potential between the water going into the pore and the water going out the pore. This effect may be found more readily among coarse-textured soils in a high-ψ domain when its mechanism is considered. Other mechanisms include the "contact-angle effect". This effect is due to the hysteresis of the contact angle between an air-water interface and a soil-solid surface. The angle generally grows when water moves toward a dry solid surface and, contrarily, closes when water recedes, as measured for soils (Letey et al., 1962) and for glass beads (Laroussi & de Backer, 1979). This effect can also induce the difference in soil water potential between a wetting process and a drying process.

Hysteresis in soil water retention has been studied mainly through laboratory experiments (e.g., Topp & Miller, 1966; Topp, 1969), while several studies that used larger soil masses have also shown that hysteretic behaviors cannot be neglected (Watson et al., 1975; Beese & van der Ploeg, 1976; Tzimas, 1979). However, so

far, limited number of studies have reported the results of multiple years of monitoring about $\psi - \theta$ relations in fields. Royer and Vachaud (1975) carried out a series of independent measurements of changes in water content and soil suction during a year, and suggested that hysteresis is too important to be ignored. Basile et al. (2003) compared laboratory- and field-measured soil water retention curves, and reported that hysteresis is essential to interpret the difference between the laboratory-measured and the field-measured soil water retention functions. However, their datasets were composed of small number of $\psi - \theta$ plots. Contrary to these studies, Li et al. (2005) reported that field measured soil water retention curves showed negligible hysteresis. As described above, knowledge about *in-situ* $\psi - \theta$ relations seems partly contradictive.

Recent studies tend to monitor *in-situ* $\psi - \theta$ relations for longer periods. Bordoni et al. (2017) monitored soil water pressure and water content in fields for 58 months. They obtained *in-situ* SWRCs for pairs of drying and wetting processes for various periods, and confirmed that soil water balance was better reproduced by considering the *in-situ* SWRCs of the two kinds of processes. Zhang et al. (2022) simulated varying soil moisture conditions for precipitation events by using field-estimated drying and wetting SWRCs, and concluded that a simulation with a field-drying SWRC and a field-wetting SWRC gave better results than that with a laboratory SWRC. Based on these studies, the likelihood is that using at least a pair of drying and wetting SWRCs gives better estimations or predictions of soil water movement in fields. And, thus, the study on soil water hysteresis is in the stage of characterizing *in-situ* hysteretic behaviors by gathering as many cases of wetting-drying cycles in soil layers as possible.

Therefore, this study probed *in-situ* $\psi - \theta$ relations for 82 months by coincidently monitoring soil water potentials ψ and volumetric water contents θ, and characterized their hysteretic behaviors. The tested soil layers were volcanic ash soil layers that are typically found in eastern part of Japan archipelago. Volcanic ash soils are also primary land-covers in areas with volcanoes like the densely populated regions along the Pacific rim.

2. Materials and Methods

2.1. Study Field

The study field was a meadow (36˚29'23"N, 139˚59'14"E) in the Utsunomiya University Farm in Moka city, Tochigi, Japan. From 2013 to 2019, Moka city had mean atmospheric temperatures of 14.0˚C, 13.6˚C, 14.3˚C, 14.1˚C, 13.5˚C, 14.7˚C, and 14.4˚C and annual precipitations of 1249, 1604, 1391, 1421, 1140, 1045, and 1458 [mm], respectively (Japan Meteorological Agency, 2024). The meadow was 2.8 ha in size with its sides of 350 m from north to south and of 80 m from east to west, along the east side of which larch tree rows (*Larix kaempferi* (Lamb.) Carr.) had stretched as a windbreak. The grasses and forbs that had grown in the meadow were orchard grass (*Dactylis glomerata* L. cv. Natsumidori), tall fescue (*Festuca arundinacea* Schreb. cv. Kentucky 31), perennial ryegrass (*Lolium pe-*

renne L. cv. Friend), and white clover (*Trifolium repens* L. cv. Huia) until July 2014. Then, the meadow was renovated for recovering yields and, in October 2014, orchard grass (*Dactylis glomerata* L. cv. Natsumidori), tall fescue (*Festuca arundinacea* Schreb. cv. Hokuryo), hybrid ryegrass (*Lolium hybridum* Hausskn. cv. Tetrelite II) and red clover (*Trifolium pratense* L. cv. Makimidori) were newly planted.

2.2. Locations for Data Sampling

Two study sites have been placed at 2- and 8-m away from the larch tree row in the study field (Figure 1). The two sites were named the sites A and B, respectively. Two data-sampling points were set at 40- and 100-cm in depth at each site. The depths were in the Kanto Loam layer which is broadly found over the Kanto Plane in Japan and is composed mainly of Pleistocene volcanic ashes (Kanto Loam Research Group, 1961). The sampling points were named "A-40", "A-100", "B-40", and "B-100", respectively. The two sites were expected to contrast the temporal behaviors in soil water potential with strong and weak plant root activities. The roots of the larch trees were found in the site A, while the site B was outside the range of tree root elongation. The grasses and forbs, on the other hand, had not had their roots go down to any of the four data-sampling points.

2.3. Measurements of Soil Water Potential ψ and Volumetric Water Content θ

Volumetric water content θ and soil water potential ψ had been coincidently measured at each of the sampling points two to three times a week from June

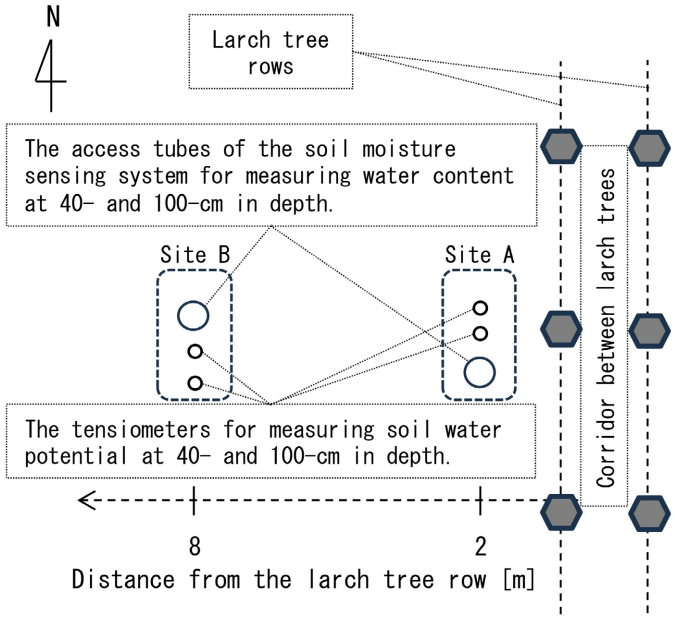

Figure 1. The description of the study sites in the meadow field in Utsunomiya University Farm.

2013 to March 2020. The values of θ were measured by using a capacitance-type soil moisture sensing system (Diviner 2000, Sentek Pty Ltd., Stepney, South Australia). This system was calibrated particularly for the study site (Iiyama, 2016). The tensiometer tubes were permanently installed to evaluate the values of ψ. And air-pressure in the head space of a tensiometer tube was measured by a digital manometer (PG-100-102VP; NIDEC COPAL Electronics Corp., Tokyo, Japan), which was converted to ψ in accordance with the height of water column in a tensiometer tube.

2.4. Measurements of Soil Physical Properties

When the devices for measuring θ and ψ were installed at each of the sampling points, triplicate undisturbed soil cores of 50 cm^3 and disturbed soil samples were taken. The soil cores were used to determine θ under −0.1, −0.98, −9.8, and −98 [$J \cdot kg^{-1}$] in ψ by applying the hanging-water-column and the pressure-plate methods (Dane & Hopmans, 2002). Soil bulk density ρ_d was also determined with the soil cores by the gravimetric method in which the soils are dried at 105˚C for more than 24 hours. Soil particle density ρ_s was measured with the disturbed soil samples in accord with Japan industrial standards "JIS A 1202" using Gay-Lussac-type pycnometers. Soil texture was also determined through the particle-size analysis (Gee & Or, 2002).

3. Results

3.1. Soil Physical Properties

Soil physical properties of the soil samples were listed in Table 1. The values of soil bulk density ρ_d ranged between 0.51 and 0.62 $Mg \cdot m^{-3}$ while the soil particle density ρ_s took the values from 2.77 to 2.84 $Mg \cdot m^{-3}$. Thus, the saturated volumetric water content θ_s were evaluated between 0.77 and 0.82 $m^3 \cdot m^{-3}$ according to the relation "$\theta_s = 1 - \rho_d/\rho_s$".

The values of θ_{pF3} indicated that more than 60% of the entire soil volume is filled with water even at $\psi = -98$ $J \cdot kg^{-1}$, though the soils nearer to the tree rows

Table 1. Soil physical properties for the sampling points. The sampling points are indicated with the site names "A" and "B" followed by the depths "40" and "100" in centimeter. The soil texture was determined as Clay Loam with the ratio of sand: silt: clay = 36:43:21 in reference to the standard of the International Union of Soil Sciences (IUSS), while it can be evaluated as 16:63:21 of Silty Loam according to the USDA standard. ρ_d and ρ_s denote bulk density and particle density, respectively. The values are averages of triplicates each followed by standard deviations in the parentheses. θ_{pF0}, θ_{pF1}, θ_{pF2}, and θ_{pF3} indicate volumetric water contents for −0.1, −0.98, −9.8, and −98 [$J \cdot kg^{-1}$] in soil water potential, respectively. Each value is an average for triplicates with a standard deviation in parentheses.

sampling points	soil texture	ρ_d [$Mg \cdot m^{-3}$]	ρ_s [$Mg \cdot m^{-3}$]	θ_{pF0} [$m^3 \cdot m^{-3}$]	θ_{pF1} [$m^3 \cdot m^{-3}$]	θ_{pF2} [$m^3 \cdot m^{-3}$]	θ_{pF3} [$m^3 \cdot m^{-3}$]
A-40	Clay Loam	0.612 (0.011)	2.836 (0.026)	0.786 (0.007)	0.736 (0.031)	0.654 (0.011)	0.610 (0.007)
A-100		0.519 (0.006)	2.808 (0.011)	0.800 (0.025)	0.762 (0.036)	0.698 (0.017)	0.650 (0.015)
B-40		0.600 (0.023)	2.811 (0.053)	0.754 (0.008)	0.734 (0.006)	0.671 (0.024)	0.609 (0.031)
B-100		0.602 (0.023)	2.777 (0.028)	0.768 (0.025)	0.739 (0.004)	0.681 (0.010)	0.651 (0.011)

were likely to be drained more easily. This feature is found commonly on a Kanto Loam layer. In general, subsoils of a Kanto Loam layer have large amount of non-free water (Takenaka, 1963) so that sometimes more than half of the pores is undrained even under a moisture condition of the permanent wilting point (Yamazaki et al., 1963). Also, large fraction of free-water is retained in poorly-continuous or dead-end macropores within the massive soil structure and, sometimes, lowering ψ to −300 J·kg^{-1} is required for draining out the free-water fraction (Takenaka et al., 1963).

3.2. Time Series of ψ and θ in the Study Field

The time-series of water potentials ψ and volumetric water contents θ are shown in **Figure 2**. The values of ψ in the sampling points A-40 and A-100 had varied broadly and dropped frequently below −10 J·kg^{-1}. As a result, the values of θ observed in the site A showed larger temporal variations, and the declines in θ on

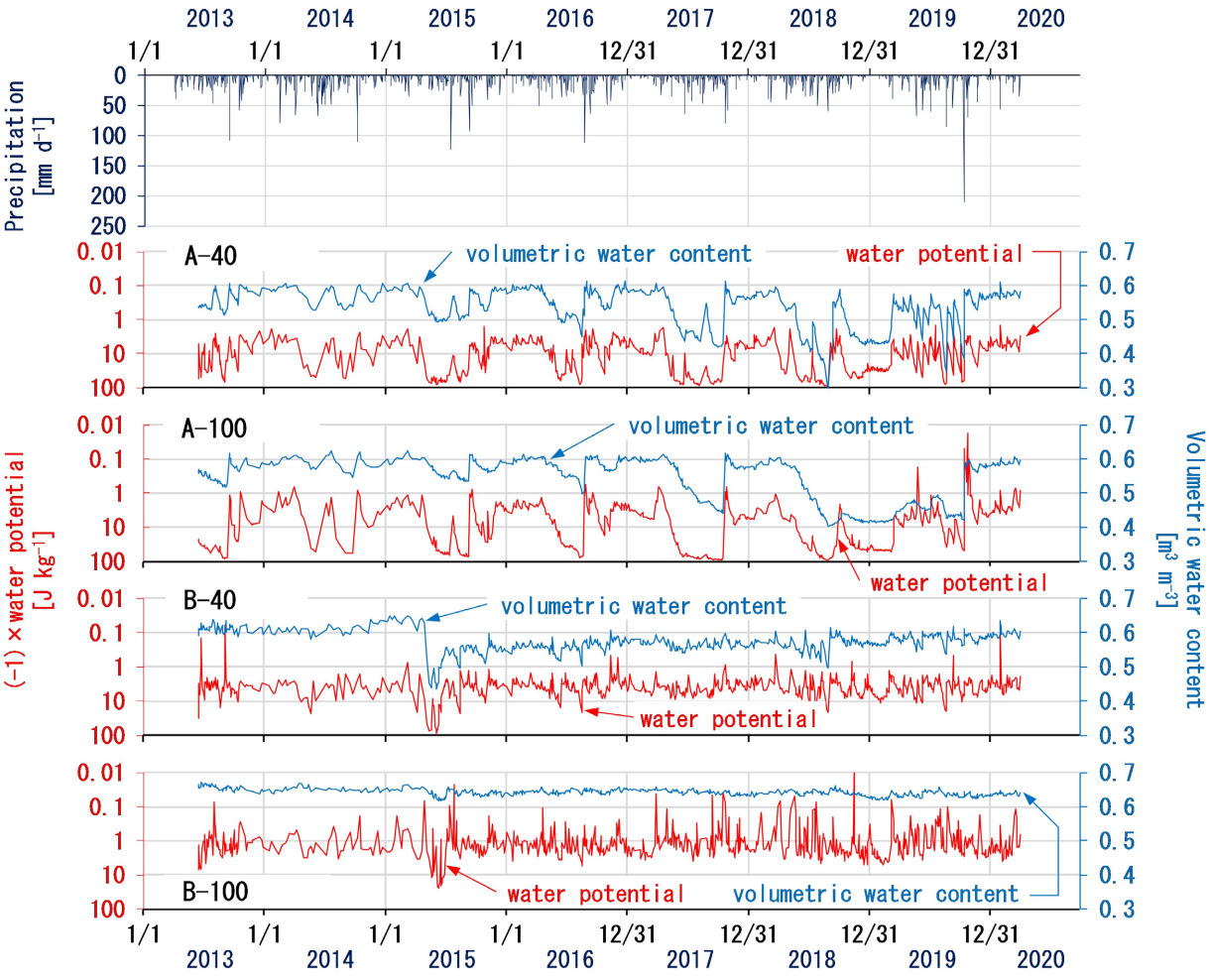

Figure 2. The time-series of water potentials and volumetric water contents monitored at the data sampling points in the study sites. Daily precipitation had been recorded at the Moka weather observation point of Japan Meteorological Agency, located 1.3-km south of the study sites. "A" or "B" in a sub-index of a sub-graph label denotes that the sub-graph is for the data set measured in either of the sites, while "40" and "100" in the sub-indices indicate the depths of monitoring in centimeter.

timescales of months occurred several times. On the other hand, the values of ψ in the sampling points B-40 and B-100 had minutely fluctuated mainly in the range above −10 $J \cdot kg^{-1}$, suggesting that the soil layers were moist on most measurement dates and their pore-water pressure easily went up in response to almost every rainfall.

In the site A, the largest reduction in θ occurred from April to August in 2018. In this period, the values of θ at A-40 and A-100 had decreased from 0.6 $m^3 \cdot m^{-3}$ to 0.4 $m^3 \cdot m^{-3}$ or less with concurrent continual declines in ψ. Particularly at A-100, θ had stayed around 0.45 $m^3 \cdot m^{-3}$ for almost one year even after ψ recovered above -10 $J \cdot kg^{-1}$. A definite chance of recovery in θ in the site A happened on October 12 in 2019 when the typhoon Hagibis passed Moka city with daily rainfall of 209.5 $mm \cdot d^{-1}$, including the recorded maximum hourly rainfall of 27.5 $mm \cdot h^{-1}$ in the study period (Japan Meteorological Agency, 2024). After that, the values of θ in the site A regained to above 0.55 $m^3 \cdot m^{-3}$.

In the site B, ψ dropped down most apparently in May in 2015. At B-40, this reduction in ψ caused the decrease in θ to less than 0.5 $m^3 \cdot m^{-3}$. After that, it took more than 4 years for this depth to restore the value of θ to around 0.6 $m^3 \cdot m^{-3}$, though the value of ψ at this depth migrated around the same level as found before 2015. At B-100, where the level of ψ was almost always higher than -10 $J \cdot kg^{-1}$, θ had never been below 0.6 $m^3 \cdot m^{-3}$ in the entire study period, suggesting that the demand for soil water at this depth had been too weak to withdraw substantial amount of soil water from the soil layer.

3.3. *In-Situ* $\psi - \theta$ Relations

Figure 3 shows the relations between soil water potential ψ and volumetric

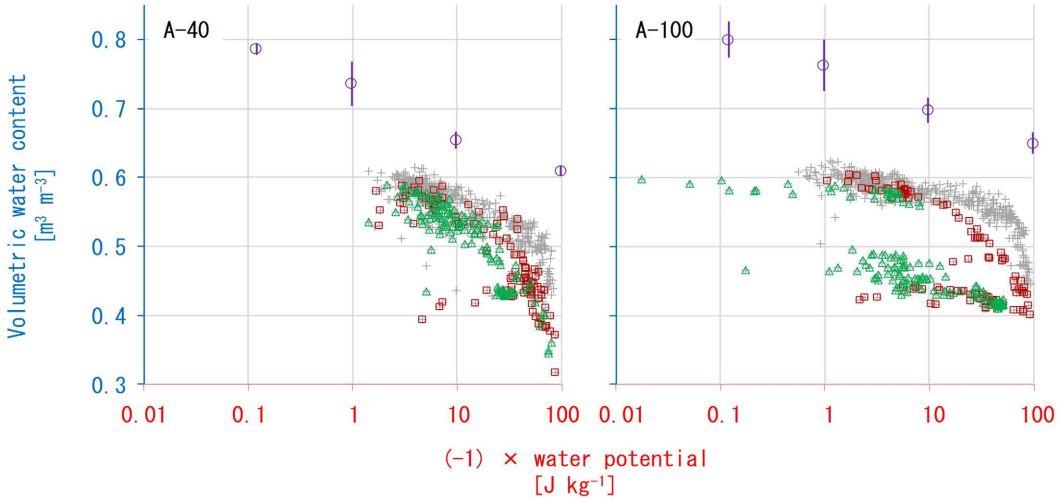

Figure 3. The relations between soil water potential and volumetric water content measured in the laboratory experiments (circles, whose values are shown in Table 1) and in the field (other types of plots) for the site A. An error bar centered at a circle spans two standard deviations among the triplicate measurements. The sub-indices "40" and "100" indicate the depths of monitoring in centimeter. The plots for the field experiment are classified into three kinds, namely, those obtained in 2018 (squares), in 2019 (triangles), and in other years (plus marks).

water content θ for the site A. Each $\psi - \theta$ plot was made by linking a value of ψ to the value of θ that was obtained with the ψ in the same sampling date. The laboratory-measured $\psi - \theta$ plots, as shown in Table 1, are also plotted in each sub-graph for the comparison between the *in-situ* and the laboratory-measured $\psi - \theta$ relations. The plots for the field experiment are classified into three groups: the plots obtained in 2018, in 2019, and in other years. This classification was aimed at clarifying the large hysteretic behavior in the $\psi - \theta$ relation, which had continued during the two years and was affected by the typhoon Hagibis.

The *in-situ* $\psi - \theta$ relations were plotted consistently in the domain lower in θ than the laboratory-measured $\psi - \theta$ relations, implying that they rarely follow the primary drying SWRC obtained through a laboratory experiment. The trajectory of the *in-situ* $\psi - \theta$ plots showed hysteretic behaviors with various size and temporal scales.

The large hysteresis observed at A-100 from 2018 to 2019 drew a clockwise loop on the graph. In the first half of 2018, the value of θ of A-100 continually decreased from 0.6 to 0.4 $m^3 \cdot m^{-3}$ with ψ going down from −1 $J \cdot kg^{-1}$ to −100 $J \cdot kg^{-1}$ and, then, stayed around 0.42 $m^3 \cdot m^{-3}$ by October in 2019. When the typhoon Hagibis passed Moka city on October 12 in 2019, the value of θ of A-100 jumped up to 0.6 $m^3 \cdot m^{-3}$, and the $\psi - \theta$ relations merged into those obtained before 2018 again. Contrary, at A-40, hysteretic behaviors were not so clearly observed as at A-100, because the value of ψ at A-40 fluctuated more frequently and minutely than that at A-100 so that the scales of wetting-drying cycles were not enough large to make a clear hysteresis loop of $\psi - \theta$ plots.

Figure 4 shows the relations between soil water potential ψ and volumetric

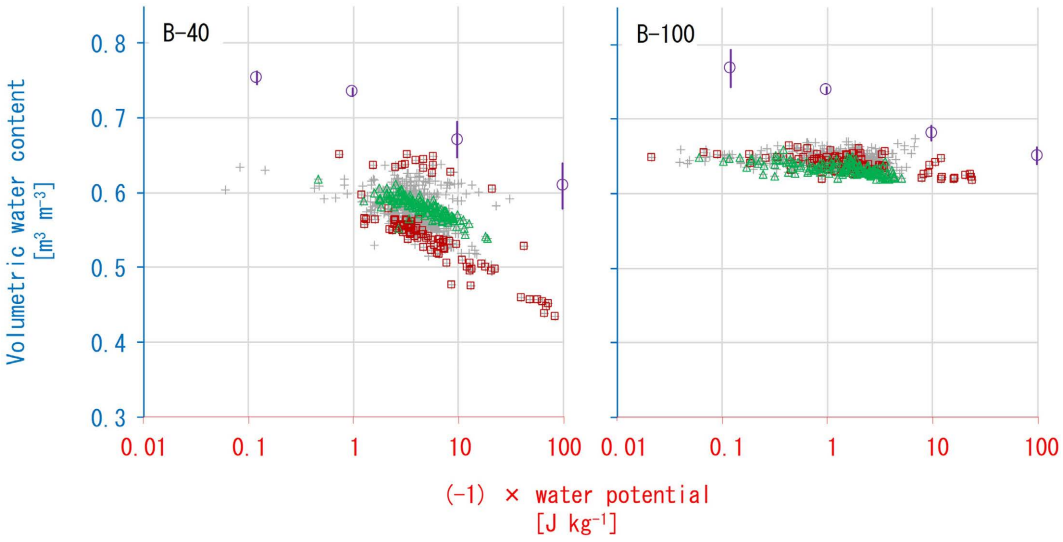

Figure 4. The relations between soil water potential and volumetric water content measured in the laboratory experiments (circles, whose values are shown in Table 1) and in the field (other types of plots) for the site B. An error bar centered at a circle spans two standard deviations among the triplicate measurements. The sub-indices "40" and "100" indicate the depths of monitoring in centimeter. The plots for the field experiment are classified into three kinds, namely, those obtained in 2015 (squares), in 2019 (triangles), and in other years (plus marks).

water content θ for the site B in the same manners as Figure 3 for the site A. The classification of the plots for the field experiment is made to distinguish the data sets obtained in 2015 and 2019 from those obtained in other years. This classification was also intended to clearly show the shift in $\psi - \theta$ relations that began in 2015. The plots for 2019 were emphasized because the value of θ at B-40 was so gradually increasing for the last 4 years in the study period that the data plots for the other years overlapped each other too much to meet the aim of this classification.

In the site B, the values of θ were ordinarily higher than those in the site A during the whole study period so that any drying process did not made progress so far as those in the site A. Particularly at B-100, θ varied within a very limited range around 0.65 $m^3 \cdot m^{-3}$ while ψ fluctuated around −1 $J \cdot kg^{-1}$. Thus, the $\psi - \theta$ relation at this depth was plotted in such a narrow band-like region on the graph, and can roughly be approximated by some single-valued function $\theta(\psi)$. At B-40, the series of $\psi - \theta$ plots showed a clockwise hysteretic spiral, instead of a loop, in 2015. In the first three weeks in May in 2015, θ decreased monotonously from 0.63 to 0.45 $m^3 \cdot m^{-3}$ while ψ lowered from −8 to −72 $J \cdot kg^{-1}$. After that, the $\psi - \theta$ relation went back and forth repeatedly in the domain of $-100\ J \cdot kg^{-1} < \psi < -1\ J \cdot kg^{-1}$ with $0.43\ m^3 \cdot m^{-3} < \theta < 0.60\ m^3 \cdot m^{-3}$ till the end of 2015. Then, the $\psi - \theta$ relation was going upward very gradually for 4 years and, as a result, the $\psi - \theta$ relation obtained in 2019 were plotted in the region obviously higher in θ than those in 2015.

4. Discussion

The facts found in Figure 3 and Figure 4 suggest that soil water hysteresis in a field cannot be ignored as some past studies referred to (Royer & Vachaud, 1975; Basile et al., 2003), once it clearly takes place as shown in A-100 and B-40. At the same time, it is also true that hysteretic behaviors of an *in-situ* $\psi - \theta$ relation may be so small as Li et al. (2005) reported that the *in-situ* $\psi - \theta$ relation can be roughly imitated by a single-valued function of $\theta(\psi)$ even for several years as shown in B-100 in Figure 4.

The sub-graphs A-100 in Figure 3 and B-40 in Figure 4 imply that the occurrence of a hysteresis loop requires difference in the slope $d\theta/d\psi$ between a drying process and a wetting process. For instance, $d\theta/d\psi$ of a drying process was steeper than that of a wetting process in a low-ψ domain like $\psi < -10\ J \cdot kg^{-1}$ at each of A-100 and B-40, and this feature made the $\psi - \theta$ relations of the two sampling points shift downward on the graphs through the wetting-drying cycles in this low-ψ domain. To restore the lowered values of θ, on the other hand, a trajectory of $\psi - \theta$ plots should be drawn in a domain of ψ where $d\theta/d\psi$ of a drying process is more gradual than that of a wetting process. Such domain of ψ was likely to be $\psi > -1\ J \cdot kg^{-1}$ at either of A-100 and B-40. Particularly at A-100, the restoration of θ to the level around 0.6 $m^3 \cdot m^{-3}$ in 2019 required ψ to regain more than −0.1 $J \cdot kg^{-1}$, suggesting that a wetting process has a very steep

$d\theta/d\psi$ in the domain of $\psi > -0.1$ J·kg^{-1}.

The observed features of how a $\psi - \theta$ relation shows hysteresis can be schematized in Figure 5. The essential features are summarized into such three assumptions as: (a1) the domain of ψ is divided into three types of sub-domain, namely, 1) the domain in which a drying process is drawn with more gradual $d\theta/d\psi$ than a wetting process, 2) the domain in which both processes have similar $d\theta/d\psi$, and 3) the domain in which a drying process is drawn with steeper $d\theta/d\psi$ than a wetting process. (a2) Any scanning curve is drawn in the region surrounded by primary drying and wetting curves. (a3) Any scanning curve has a similar figure of a corresponding primary curve, and is asymptotically merging into the corresponding primary curve until the process will reverse its direction.

On these assumptions, the factors affecting how hysteretic behavior of a $\psi - \theta$ relation appears should be (f1) the width of each of the domains of ψ, and (f2) the size of difference in $d\theta/d\psi$ between drying and wetting processes in each of the domains of ψ. For example, when a soil has a broad domain- (ii), soil water hysteresis of the soil should become apparently negligible when wetting-drying cycles of the soil are repeated well within the domain- (ii) as found at B-100 in this study ("ex1" in Figure 5).

On the other hand, when wetting-drying cycles are repeated solely in the domain- (iii), a $\psi - \theta$ relation should gradually shift downward on the graph, and finally, can be found migrating around the primary wetting curve as shown at A-100 and B-40 in this study ("ex2" in Figure 5). The depletion in θ caused by

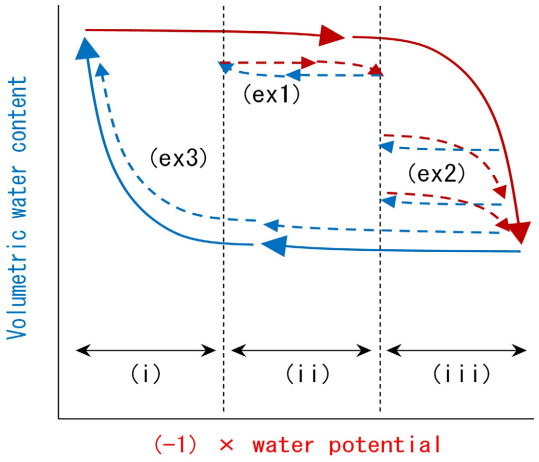

Figure 5. A schematic diagram of how a $\psi - \theta$ relation shows hysteresis with the assumptions as follows: (a1) the domain of ψ is divided into three types of sub-domain, namely, (i) the domain in which a drying process is drawn with more gradual $d\theta/d\psi$ than a wetting process, (ii) the domain in which the values of $d\theta/d\psi$ of both processes are like each other, and (iii) the domain in which a drying process is drawn with steeper $d\theta/d\psi$ than a wetting process. (a2) Any scanning curve is drawn in the region surrounded by primary drying and wetting curves. (a3) Any scanning curve is a similitude of a corresponding primary curve, and the ratio of the similitude is determined probably by the distance in the direction of θ between the scanning curve and the corresponding primary curve. Three examples of wetting-drying processes that may occur on these assumptions are presented as "ex1", "ex2", and "ex3" on the graph.

this type of downward shift in $\psi - \theta$ relation can be restored when the soil experiences a wetting process that reaches the domain- (i) as observed at A-100 ("ex3" in Figure 5).

A large hysteretic loop can emerge when a $\psi - \theta$ relation passes both the domain- (i) and the domain- (iii), namely, when both a demand for soil water strong enough to make ψ go into the domain- (iii) and a water supply to the soil intense enough to regain ψ to the domain- (i) occur. And it is likely that hysteresis loops appear more clearly in a soil that has SWRCs with larger difference in $d\theta/d\psi$ between the wetting and drying processes in any of the domain- (i) and the domain- (iii).

A volcanic ash soil as used in this study is likely to be typical of a soil with a broad domain- (ii) and, thus, can show an apparently "hysteresis-less" $\psi - \theta$ relation for years. A $\psi - \theta$ relation for a soil with a narrow domain- (ii), on the other hand, is expected to shift more frequently toward a moister or a dryer region of θ. In addition, a soil in a climatic region with more distinct a pair of rainy season and dry season in a year may have a $\psi - \theta$ relation with more drastic soil water hysteresis.

These expectations should be confirmed with further collections of *in-situ* $\psi - \theta$ relations for various combinations of soil types and climatic zones. Particularly, knowledge about wetting SWRCs, in addition to drying SWRCs, should be accumulated to analyze and predict soil water regimes in fields in more precise manners. At the same time, how often large hysteresis loops are clearly drawn depends on how frequently the land encounters extreme weather conditions. So, it is also necessary to gain our understandings about the long-term trends of frequencies of extreme weather conditions associated with possible change in climate.

5. Conclusion

For characterizing hysteretic behaviors of *in-situ* $\psi - \theta$ relations, soil water potentials ψ and volumetric water contents θ had been monitored coincidently in a meadow field for 82 months. The tested soil layers were volcanic ash soil layers, as an example of primary land-covers in areas with volcanoes like the densely populated regions along the Pacific rim. Laboratory-measured $\psi - \theta$ relations were also obtained by using undisturbed soil samples for the comparison with the *in-situ* $\psi - \theta$ relations.

The *in-situ* $\psi - \theta$ relations were plotted consistently in the domain lower in θ than the laboratory-measured $\psi - \theta$ relations, implying that *in-situ* $\psi - \theta$ plots mostly follow scanning SWRCs and rarely follow the primary drying SWRC.

Large hysteretic behaviors in the *in-situ* $\psi - \theta$ relations were observed a few times during the study period. The large hysteretic behaviors began with unusually strong continual reductions in ψ. Once the value of θ decreased significantly by the strong continual reduction in ψ, the *in-situ* $\psi - \theta$ relation tended to reside in a low-θ region on the $\psi - \theta$ graph. To complete a hysteresis loop, a

recorded maximum rainfall was required. In the sampling depth that had not experienced such a large amount of water supply in a short period, the $\psi - \theta$ relation failed to complete a loop and, instead, had developed a spiral trajectory on a $\psi - \theta$ graph for at least four years. In either way, it was suggested that it will take many years to recover a loss of soil water once a significant fraction of soil water is depleted by an unusually strong continual reduction in ψ. In case that wetting-drying cycles had occurred solely within a certain domain of ψ during the entire study period, hysteretic behaviors were so small that the *in-situ* $\psi - \theta$ relation can be modeled by a single-valued function of $\theta(\psi)$.

This study simplified the features of soil water hysteresis into the following three assumptions: (a1) The domain of ψ is divided into three types of sub-domain, namely, (i) the domain with a drying process of gradual $d\theta/d\psi$ and a wetting process of steep $d\theta/d\psi$, (ii) the domain of an apparently "hysteresis-less" $\psi - \theta$ relation, and (iii) the domain with a drying process of steep $d\theta/d\psi$ and a wetting process of gradual $d\theta/d\psi$. (a2) Any scanning curve is drawn inside the loop of primary drying and wetting curves. (a3) Any scanning curve has a similar figure of a corresponding primary curve, and is asymptotically merging into the corresponding primary curve until the process will reverse its direction.

These features of soil water hysteresis suggest that the factors affecting how hysteretic behavior of a $\psi - \theta$ relation appears should be (f1) the width of each of the domains of ψ, and (f2) the size of difference in $d\theta/d\psi$ between drying and wetting processes in each of the domains of ψ. To confirm these characterizations, more amounts of experimental facts about wetting SWRCs, in addition to drying SWRCs, should be accumulated to analyze and predict soil water regimes in fields in more precise manners. At the same time, it is also necessary to increase our understandings about the long-term trends of occurrences of extreme weather conditions associated with possible change in climate, since the frequency of large drying- or wetting-shifts in an *in-situ* $\psi - \theta$ relation must depend on the frequency of extreme weather conditions that the field encounters.

Acknowledgements

The author thanks Mr. T. Shiozawa, Mr. E. Saito, Mr. K Seino, and Mr. N. Yamaguchi at the Utsunomiya University Farm who have managed the study field. The author also thanks Mr. T. Hirai of the former student in the Graduate school of Agriculture, Utsunomiya University, and Mr. H. Ajito, Ms. M. Anzai, Ms. K. Arakawa, Ms. M. Cho, Ms. N. Goka, Mr. T. Hoshino, Mr. D. Iimura, Mr. J. Kaneko, Mr. T. Kurata, Mr. K. Ogasawara, Mr. Y. Sakanishi, Mr. H. Shoji, Mr. H. Suto, Mr. S. Takaki, Mr. K. Tezuka, Mr. N. Totsuka, Mr. K. Tsukagoshi, and Mr. Y. Usui of the former students in the Faculty of Agriculture, Utsunomiya University, for their works in the field and in the laboratory.

Conflicts of Interest

The author declares no conflicts of interest regarding the publication of this paper.

References

Basile, A., Ciollaro, G., & Coppola, A. (2003). Hysteresis in Soil Water Characteristics as a Key to Interpreting Comparisons of Laboratory and Field Measured Hydraulic Properties. *Water Resources Research*, 39, 1355. https://doi.org/10.1029/2003WR002432

Beese, F., & van der Ploeg, R. R. (1976). Influence of Hysteresis on Moisture Flow in an Undisturbed Soil Monolith. *Soil Science Society of America Journal, 40,* 480-484. https://doi.org/10.2136/sssaj1976.03615995004000040012x

Bordoni, M., Bittelli, M., Valentino, R., & Meisina, C. (2017). Improving the Estimation of Complete Field Soil Water Characteristic Curves through Field Monitoring Data. *Journal of Hydrology, 552,* 283-305. https://doi.org/10.1016/j.jhydrol.2017.07.004

Campbell, G. S. (1974). A Simple Method for Determining Unsaturated Conductivity from Moisture Retention Data. *Soil Science, 117,* 311-314. https://doi.org/10.1097/00010694-197406000-00001

Clapp, R. B., & Hornberger, G. M. (1978). Empirical Equations for Some Soil Hydraulic Properties. *Water Resources Research, 14,* 601-604. https://doi.org/10.1029/WR014i004p00601

Dane, J. H., & Hopmans, J. W., (2002). Water Retention and Storage. In J. H. Dane, & G. C. Topp (Eds.), *Methods of Soil Analysis: Part 4, Physical Methods* (pp. 680-683). Soil Science Society of America.

Gee, G. W., & Or, D. (2002). Particle-Size Analysis. In J. H. Dane, & G. C. (Eds.), *Methods of Soil Analysis: Part 4, Physical Methods* (pp. 255-293). Soil Science Society of America. https://doi.org/10.2136/sssabookser5.4.c12

Haines, W. B. (1930). Studies in the Physical Properties of Soils. V. The Hysteresis Effect in Capillary Properties and the Modes of Moisture Distribution Associated Therewith. *The Journal of Agricultural Science, 20,* 97-116. https://doi.org/10.1017/S002185960008864X

Hillel, D. (1998). *Environmental Soil Physics* (pp. 159-161). Academic Press.

Hoover, M. D. (1950). Hydrologic Characteristics of South Carolina Piedmont Forest Soils. *Soil Science Society of America Proceedings, 14,* 353-358. https://doi.org/10.2136/sssaj1950.036159950014000C0083x

Iiyama, I. (2016). Differences between Field-Monitored and Laboratory-Measured Soil Moisture Characteristics. *Soil Science and Plant Nutrition, 62,* 416-422. https://doi.org/10.1080/00380768.2016.1242367

Japan Meteorological Agency (2024). *Weather Station Data in Moka City in Utsunomiya Local Meteorological Office.* http://www.jma.go.jp/jma/en/quickinfo/quickinfo.html

Kanto Loam Research Group (1961). The Kanto Loam and the Quaternary Chronology of the Kanto District, Japan. *Earth Science: Journal of the Association for the Geological Collaboration in Japan, 54,* 20-29.

Kutilek, M., & Nielsen, D. R. (1994). *Soil Hydrology* (pp. 70-73). Cremlingen-Destedt.

Laroussi, C., & de Backer, L. W. (1979). Relations between Geometrical Properties of Glass Beads Media and Their Main $\psi(\theta)$ Hysteresis Loops. *Soil Science Society of America Journal, 43,* 646-650. https://doi.org/10.2136/sssaj1979.03615995004300040004x

Letey, J., Osborn, J., & Pelishek, R. E. (1962). Measurement of Liquid-Solid Contact Angles in Soil and Sand. *Soil Science, 93,* 149-153. https://doi.org/10.1097/00010694-196203000-00001

Li, A. G., Tham, L. G., Yue, Z. Q., Lee, C. F., & Law, K. T. (2005). Comparison of Field and Laboratory Soil-Water Characteristic Curves. *Journal of Geotechnical and Geoenvironmental Engineering, 131,* 1176-1180.

https://doi.org/10.1061/(ASCE)1090-0241(2005)131:9(1176)

Richards, L. A., & Weaver, L. R. (1943). Fifteen-Atmosphere Percentages as Related to the Permanent Wilting Percentage. *Soil Science, 56,* 331-340. https://doi.org/10.1097/00010694-194311000-00002

Royer, J. M., & Vachaud, G. (1975). Field Determination of Hysteresis in Soil Water Characteristics. *Soil Science Society of America Proceedings, 39,* 221-223. https://doi.org/10.2136/sssaj1975.03615995003900020006x

Takenaka, H. (1963). On the Characteristics of Non-Free Water of the Kanto Loam Volcanic Ash Soil. *Transactions of the Japanese Society of Irrigation, Drainage and Reclamation Engineering (Nougyou Doboku Kenkyu Bessatsu), 7,* 68-75. (In Japanese)

Takenaka, H., Tabuchi, T., Tabuchi, K., & Tada, A., (1963). Studies on the Free Water of the Kanto Loam Volcanic Ash Soil. *Transactions of the Japanese Society of Irrigation, Drainage and Reclamation Engineering (Nougyou Doboku Kenkyu Bessatsu), 7,* 61-67. (In Japanese)

Topp, G. C. (1969). Soil Water Hysteresis Measured in a Sandy Loam Compared with the Hysteresis Domain Model. *Soil Science Society of America Proceedings, 33,* 645-651. https://doi.org/10.2136/sssaj1969.03615995003300050011x

Topp, G. C., & Miller, E. E. (1966). Hysteresis Moisture Characteristics and Hydraulic Conductivities for Glass-Bead Media. *Soil Science Society of America Proceedings, 30,* 156-162. https://doi.org/10.2136/sssaj1966.03615995003000020008x

Tzimas, E. (1979). The Measurement of Soil Water Hysteresis Relationships on a Soil Monolith. *Journal of Soil Science, 30,* 529-534. https://doi.org/10.1111/j.1365-2389.1979.tb01006.x

van Genuchten, M. T. (1980). A Closed-Form Equation for Predicting the Hydraulic Conductivity of Unsaturated Soils. *Soil Science Society of America Journal, 44,* 892-898. https://doi.org/10.2136/sssaj1980.03615995004400050002x

Veihmeyer, F. J., & Hendrickson, A. H. (1931). The Moisture Equivalent as a Measure of the Field Capacity of Soils. *Soil Science, 32,* 181-193. https://doi.org/10.1097/00010694-193109000-00003

Veihmeyer, F. J., & Hendrickson, A. H. (1948). The Permanent Wilting Percentage as a Reference for the Measure of Soil Moisture. *Transactions American Geophysical Union, 29,* 887-896. https://doi.org/10.1029/TR029i006p00887

Washburn, E. W. (1921). Note on a Method of Determining the Distribution of Pore Sizes in A Porous Material. *Proceedings of the National Academy of Sciences of the United States of America, 7,* 115-116. https://doi.org/10.1073/pnas.7.4.115

Watson, K. K., Reginato, R. J., & Jackson, R. D. (1975). Soil Water Hysteresis in a Field Soil. *Soil Science Society of America Proceedings, 39,* 242-246. https://doi.org/10.2136/sssaj1975.03615995003900020010x

Yamazaki, F., Yawata., T., & Sudo, S. (1963). Physical Properties of the Kanto Loam. *Transactions of the Japanese Society of Irrigation, Drainage and Reclamation Engineering (Nougyou Doboku Kenkyu Bessatsu), 7,* 1-13. (In Japanese)

Zhang, P., Chen, G., Wu, J., Wang, C., Zheng, S., Yu, Y., Li, Y., & Li, X. (2022). The Application and Improvement of Soil-Water Characteristic Curves through *in Situ* Monitoring Data in the Plains. *Water, 14,* Article 4012. https://doi.org/10.3390/w14244012